Article:
Crook, JA, Forster, PM and Stuber, N (2011) Spatial Patterns of Modeled Climate Feedback and Contributions to Temperature Response and Polar Amplification. Journal of Climate, 24 (14). 3575 - 3592 . ISSN 0894-8755

https://doi.org/10.1175/2011JCLI3863.1

Spatial Patterns of Modeled Climate Feedback and Contributions to Temperature Response and Polar Amplification

JULIA A. CROOK AND PIERS M. FORSTER

School of Earth and Environment, University of Leeds, Leeds, United Kingdom

NICOLA STUBER

Department of Meteorology, University of Reading, Reading, United Kingdom

(Manuscript received 19 May 2010, in final form 10 February 2011)

ABSTRACT

Spatial patterns of local climate feedback and equilibrium partial temperature responses are produced from eight general circulation models with slab oceans forced by doubling carbon dioxide (CO_2). The analysis is extended to other forcing mechanisms with the Met Office Hadley Centre slab ocean climate model version 3 (HadSM3). In agreement with previous studies, the greatest intermodel differences are in the tropical cloud feedbacks. However, the greatest intermodel spread in the equilibrium temperature response comes from the water vapor plus lapse rate feedback, not clouds, disagreeing with a previous study. Although the surface albedo feedback contributes most in the annual mean to the greater warming of high latitudes, compared to the tropics (polar amplification), its effect is significantly ameliorated by shortwave cloud feedback. In different seasons the relative importance of the contributions varies considerably, with longwave cloudy-sky feedback and horizontal heat transport plus ocean heat release playing a major role during winter and autumn when polar amplification is greatest. The greatest intermodel spread in annual mean polar amplification is due to variations in horizontal heat transport and shortwave cloud feedback. Spatial patterns of local climate feedback for HadSM3 forced with $2 \times CO_2$, +2% solar, low-level scattering aerosol and high-level absorbing aerosol are more similar than those for different models forced with $2 \times CO_2$. However, the equilibrium temperature response to high-level absorbing aerosol shows considerably enhanced polar amplification compared to the other forcing mechanisms, largely due to differences in horizontal heat transport and water vapor plus lapse rate feedback, with the forcing itself acting to reduce amplification. Such variations in high-latitude response between models and forcing mechanisms make it difficult to infer specific causes of recent Arctic temperature change.

1. Introduction

Complex three-dimensional general circulation climate models (GCMs) are extensively used to make projections of temperature change due to radiative forcings such as that caused by a doubling of CO_2. Different climate models give a wide range of global mean equilibrium surface temperature responses and the likely range of 2°–4.5°C of warming for a doubling of CO_2 has little changed from previous Intergovernmental Panel on Climate Change (IPCC) reports to the latest (Meehl et al. 2007) despite model improvements. This range principally arises from differences in internal processes that either amplify or dampen the response to the external forcing (climate feedbacks). Any process that responds to temperature change and directly or indirectly affects the radiative balance may be considered a feedback. Feedback studies have mostly concentrated on quantifying the global mean feedbacks due to changes in surface albedo, water vapor, lapse rate, and clouds (e.g., Bony et al. 2006). A number of studies have looked at the spatial pattern of feedback strength, but these have generally been either an assessment of multiple feedbacks in one model (e.g., Colman 2002; Boer and Yu 2003), an assessment of one feedback in multiple models (e.g., Winton 2006a), and/or application of a new method to estimate feedback patterns (e.g., Soden et al. 2008; Winton 2006a). They also

Corresponding author address: Julia Crook, School of Earth and Environment, University of Leeds, Leeds, LS2 9JT, United Kingdom.
E-mail: j.crook@see.leeds.ac.uk

DOI: 10.1175/2011JCLI3863.1

usually assess the local contribution to the global mean feedback rather than the local feedback itself.

A number of methods have previously been used to determine feedback parameters (Bony et al. 2006). These vary in how they determine the radiation change due to a particular feedback, but they may also be affected by the definition of forcing used. It has been shown that in the global mean to first order there is a linear relationship between radiative forcing F and equilibrium surface temperature response $\Delta T_{s,\mathrm{eq}}$, such that $\Delta T_{s,\mathrm{eq}} = \lambda F$ (Forster et al. 2007). The proportionality constant λ is known as the climate sensitivity parameter and its negative inverse $Y = -1/\lambda$, as the "signed" climate feedback parameter (taking the negative means that Y is a negative number representing an overall negative feedback). The radiative forcing is generally taken as that at the tropopause or top of atmosphere (TOA) after the stratosphere has been allowed to adjust to radiative equilibrium (Forster et al. 2007). However, a number of studies have shown that the climate sensitivity parameter calculated using this standard definition of forcing varies considerably for different forcing mechanisms, particularly when the forcing pattern is geographically inhomogeneous, such as changes in ozone and absorbing aerosol (Hansen et al. 1997; Forster et al. 2000; Joshi et al. 2003; Shine et al. 2003; Forster et al. 2007). Absorption of radiation by absorbing aerosols leads to local heating, altering the vertical temperature, humidity, and cloud profiles. These relatively rapid adjustments to the troposphere cause TOA radiative flux adjustments before the surface temperature changes, which, therefore, may be considered part of the forcing rather than the feedback. Rapid tropospheric adjustments have also been found in CO_2 forcing (Gregory and Webb 2008; Andrews and Forster 2008), although these are smaller than those seen for absorbing aerosols. When the troposphere-adjusted forcing is used, the climate sensitivity parameter is generally much more constant for different forcing mechanisms (Shine et al. 2003; Hansen et al. 2005; Forster et al. 2007). Differences in the climate sensitivity parameter are then due to differences in the pattern of feedback related to different mean climate states and differences in the local contribution to the global mean feedback. The troposphere-adjusted forcing can be calculated from fixed sea surface temperature integrations (Hansen et al. 2005), fixed sea and land surface temperature integrations (Shine et al. 2003), or a regression method (Gregory et al. 2004). Regression of the radiative flux changes against the surface temperature change over the period when the climate is adjusting (Gregory et al. 2004; Forster and Taylor 2006; Gregory and Webb 2008, Andrews and Forster 2008; Williams et al. 2008) gives a slope of Y and an intercept of F_{regr}, the troposphere-adjusted forcing.

Observations suggest that the Arctic has warmed at twice the rate of the global mean over the last 100 years (Trenberth et al. 2007). All climate models from the World Climate Research Programme (WCRP) Coupled Model Intercomparison Project phase 3 (CMIP3) also show greater surface temperature response at high latitudes than low latitudes. However, the extent of this polar amplification varies considerably, with the range between the coupled ocean–atmosphere models of simulated transient Arctic warming at the point of doubling of CO_2 being 1.5 to 4.5 times the global mean (Holland and Bitz 2003). It has been shown that, although the snow and ice feedbacks play an important role in polar amplification, other feedback processes also play a part (Forster et al. 2000; Hall 2004; Alexeev et al. 2005; Cai 2006; Winton 2006b; Cai and Lu 2007; Lu and Cai 2009a; Graversen and Wang 2009). However, the relative contributions of these feedbacks to polar amplification and why it varies between models is not fully understood.

In this study, we determine the spatial pattern of local feedback using the regression method of Gregory et al. (2004) from eight slab ocean CMIP3 climate models, forced with doubled CO_2. We break down the equilibrium surface temperature response pattern for each model into components due to each feedback, the horizontal transport of heat, and the troposphere-adjusted forcing. We also quantify the contribution of these components to polar amplification. We apply the same analysis to the results from idealized aerosol perturbation experiments as well as $2 \times CO_2$ and +2% solar constant experiments using the HadSM3 GCM to investigate how feedback patterns vary between forcing mechanisms.

Our methods are described in section 2. The data for the CMIP3 models and our Hadley Centre slab ocean climate model version 3 (HadSM3) experiments are presented in sections 3a and 3b, respectively. The results are described in section 4, and final conclusions are given in section 5.

2. Methods

a. Determination of local feedback

The vertically integrated energy budget is given by

$$\frac{d\Delta H}{dt} = \Delta A + \Delta R, \tag{1}$$

where $d\Delta H/dt$ is the rate of change of energy content of the column, that is, heat storage, ΔA is the change in horizontal heat convergence, and ΔR is the change in TOA net downward radiative flux. Here, ΔR can approximated as a forcing term F and a feedback term,

which in turn can be approximated as a linear function of the surface temperature response ΔT_s, with the proportionality constant being the climate feedback parameter Y:

$$\Delta R \approx F + Y\Delta T_s. \quad (2)$$

All terms in Eqs. (1) and (2) are functions of time and space, although we assume that the feedback parameter does not change with time. Under large surface temperature responses it is likely that the feedback parameter will change, for example, once most of the snow and ice has gone the albedo feedback would reduce dramatically.

As in the cloud radiative forcing (CRF) method (Cess et al. 1990, 1996), we decompose Eq. (2) into longwave and shortwave components and then further into clear-sky and cloudy-sky (all-sky minus clear-sky) components giving longwave clear-sky (LWCS) and cloudy-sky (LWCRF) and shortwave clear-sky (SWCS) and cloudy-sky (SWCRF) feedback parameters (see also Gregory and Webb 2008):

$$\Delta R_{\mathrm{SW}} + \Delta R_{\mathrm{LW}} \approx F_{\mathrm{SW}} + F_{\mathrm{LW}} + Y_{\mathrm{SW}}\Delta T_s + Y_{\mathrm{LW}}\Delta T_s, \quad (3)$$

where

$$\Delta R_{\mathrm{SW}} = \Delta R_{\mathrm{SWCS}} + \Delta R_{\mathrm{SWCRF}} \quad \text{and}$$
$$\Delta R_{\mathrm{LW}} = \Delta R_{\mathrm{LWCS}} + \Delta R_{\mathrm{LWCRF}}; \quad \text{and}$$

$$\Delta R_{\mathrm{SWCS}} = F_{\mathrm{SWCS}} + Y_{\mathrm{SWCS}}\Delta T_s, \quad (4)$$

$$\Delta R_{\mathrm{SWCRF}} = F_{\mathrm{SWCRF}} + Y_{\mathrm{SWCRF}}\Delta T_s, \quad (5)$$

$$\Delta R_{\mathrm{LWCS}} = F_{\mathrm{LWCS}} + Y_{\mathrm{LWCS}}\Delta T_s, \quad \text{and} \quad (6)$$

$$\Delta R_{\mathrm{LWCRF}} = F_{\mathrm{LWCRF}} + Y_{\mathrm{LWCRF}}\Delta T_s. \quad (7)$$

The feedback parameter for shortwave clear sky is mostly due to the surface albedo feedback with a small negative contribution from water vapor changes. The longwave clear-sky feedback parameter is due to the water vapor and lapse rate feedbacks as well as the Planck feedback (due to Stefan–Boltzmann blackbody emission). The shortwave and longwave cloudy-sky feedbacks are mainly due to changes in cloud amount and properties. However, masking effects where noncloud feedbacks depend on whether the sky is cloudy or not (Zhang et al. 1994; Colman 2003; Soden et al. 2004) mean that part of the diagnosed cloudy-sky feedback should really be considered part of the clear-sky feedback.

An alternative way to split the shortwave component is to use the method of Winton (2006a). This estimates the shortwave flux change due to the change in surface albedo $\Delta R_{\mathrm{Alb\_f}}$ using a parameterization of the relationship between planetary and surface albedo. From this we can determine the surface albedo feedback:

$$\Delta R_{\mathrm{Alb\_f}} \approx Y_{\mathrm{Alb}}\Delta T_s. \quad (8)$$

Assuming that water vapor feedback effects on shortwave radiation are minimal, the difference between the total shortwave radiative flux change and this surface albedo radiative flux change gives the shortwave forcing component plus the shortwave radiative flux change associated with cloud changes, and therefore, can be used to find a true shortwave cloud feedback:

$$\Delta R_{\mathrm{SW}} - \Delta R_{\mathrm{Alb\_f}} \approx F_{\mathrm{SW}} + Y_{\mathrm{SWCL}}\Delta T_s. \quad (9)$$

The difference between the shortwave clear-sky feedback and the surface albedo feedback can be used to give a measure of the shortwave cloud-masking effect.

The local feedback parameters and troposphere-adjusted forcing components were determined using Eqs. (4)–(9) applied at different spatial scales by performing a linear regression of each local ΔR component against the local ΔT_s for the years before equilibrium is reached, following the method of Gregory et al. (2004). Regressions were performed on the global means, the polar regions (60°–90°N and 60°–90°S), the tropics (30°S–30°N), and the zonal means at the resolution of the model for both annual means and seasonal means, and on each 10° × 10° grid box for annual means. Regressions at all spatial scales were also performed on the total radiative flux change to find a total feedback parameter and total troposphere-adjusted forcing [Eq. (3)]. This allowed us to check that the total feedback and forcing were the same as the sum of the feedback and forcing components. We discuss the validity of linear regression at different spatial scales in section 4a. Local feedback parameters were also calculated using Eqs. (4)–(9) at equilibrium and the stratosphere-adjusted forcing components where they were available. The results from the two forcing definitions are compared in section 4b.

The longwave clear-sky feedback is further broken down into a Planck feedback term and a water vapor plus lapse rate feedback term:

$$\Delta R_{\mathrm{LWCS}} = F_{\mathrm{LWCS}} + (Y_{\mathrm{WV+LR}} + Y_{\mathrm{Planck}})\Delta T_s. \quad (10)$$

The Planck feedback term was determined by a partial radiative perturbation (PRP) method using the Edwards Slingo radiative transfer code as employed in Rap et al.

(2010). Three-dimensional temperature and specific humidity profiles were obtained for each model using the climatological monthly mean from the control run and the equilibrium monthly mean from the $2 \times CO_2$ run. For the control case the temperature was uniformly incremented by 1, 2, 3, and 4 K and the corresponding change in longwave TOA radiative flux was obtained under clear-sky conditions. For the $2 \times CO_2$ case the temperature was uniformly decremented by 1, 2, 3, and 4 K and the corresponding change in longwave TOA radiative flux was obtained under clear-sky conditions. The Planck feedback parameters for the control and $2 \times CO_2$ cases were determined by regressing the change in TOA radiative flux against the uniform temperature change. The mean of these two values was taken as the Planck feedback acting during the $2 \times CO_2$ simulation. We used regression to check that the Planck feedback was constant over the range of temperature responses typically seen in the $2 \times CO_2$ experiments. We found the Planck feedback for the $2 \times CO_2$ case was slightly less negative than that for the control case. This is because in our PRP method we are incrementing the temperature in the control above the tropical equilibrium $2 \times CO_2$ temperature and likewise decrementing the temperature in the equilibrium $2 \times CO_2$ below the tropical control temperature and we would expect Planck feedback to be more negative at higher temperatures. The greatest difference (0.1 W m^{-2} K^{-1}, i.e., ~2.5%) was found in the tropics where the surface temperature response to $2 \times CO_2$ is smallest.

The Planck feedback is strongly negative and dominates the other feedbacks giving an overall negative feedback, allowing the radiative response to oppose the forcing and a new equilibrium to be reached. At equilibrium, $d\Delta H/dt$ goes to zero in the annual mean and in the global mean ΔA goes to zero, leaving us with $\overline{F} = -\overline{Y \Delta T_{s,\mathrm{eq}}}$ where the overbar indicates a global mean. In other words, $Y_{\mathrm{gm}} = \overline{Y \Delta T_{s,\mathrm{eq}}}/\overline{\Delta T_{s,\mathrm{eq}}}$, or the local contribution to the global mean feedback is equal to the local feedback weighted by the local equilibrium surface temperature response.

b. Determination of equilibrium partial temperature changes

The energy balance Eq. (1) combined with Eqs. (3)–(9) (see also Lu and Cai 2009b) can be used to determine local partial temperature changes due to each feedback, horizontal heat transport, heat storage, and the forcing:

$$\frac{d\Delta H}{dt} - \Delta A = F + \Delta R_{\mathrm{Alb\_f}} + \Delta R_{\mathrm{SWCL\_f}} + \Delta R_{\mathrm{Planck}} + \Delta R_{\mathrm{WV+LR\_f}} + \Delta R_{\mathrm{LWCRF\_f}}, \quad (11)$$

where $\Delta R_{\mathrm{Alb\_f}}$, $\Delta R_{\mathrm{SWCL\_f}}$, $\Delta R_{\mathrm{Planck}}$, $\Delta R_{\mathrm{WV+LR\_f}}$, and $\Delta R_{\mathrm{LWCRF\_f}}$ are the changes in radiative flux due to the surface albedo feedback, the shortwave cloud (Winton) feedback, the Planck feedback, the water vapor plus lapse rate feedback, and the longwave cloudy-sky (CRF) feedback, respectively, and for each feedback $\Delta R_{\mathrm{i\_f}} = \Delta R_{\mathrm{i}}\text{-}F_{\mathrm{i}} \approx Y_{\mathrm{i}} \Delta T_{\mathrm{s}}$. After replacing $\Delta R_{\mathrm{Planck}}$ with $Y_{\mathrm{planck}} \Delta T_{\mathrm{s}}$, where Y_{Planck} is the Planck feedback parameter determined earlier, and rearranging Eq. (11) we obtain

$$\Delta T_s = \frac{-1}{Y_{\mathrm{Planck}}}\left(-\frac{d\Delta H}{dt} + \Delta A + F + \Delta R_{\mathrm{Alb\_f}} + \Delta R_{\mathrm{SWCL\_f}} + \Delta R_{\mathrm{WV+LR\_f}} + \Delta R_{\mathrm{LWCRF\_f}}\right). \quad (12)$$

The terms on the right-hand side therefore give the partial temperature changes due to the release of heat stored, the change in horizontal heat transport, the forcing, and the feedbacks. At equilibrium in the annual mean, $d\Delta H/dt$ goes to zero and the ΔR term becomes entirely due to the change in horizontal heat transport.

The equilibrium partial temperature changes for the feedbacks were calculated from $\Delta R_{\mathrm{i\_f}} = \Delta R_{\mathrm{i}}\text{-}F_{\mathrm{i}}$ using the archived stratosphere-adjusted forcing (where available) and the forcing obtained from regressions F_{regr}. The standard deviations in these equilibrium partial temperature changes from regression were calculated from the standard deviation of the corresponding F_{regr} component.

c. Determination of polar amplification contributions

Polar amplification was quantified by Holland and Bitz (2003) for the Northern Hemisphere (NH) as the mean temperature response poleward of 75°N divided by the global mean temperature response. There is no strict definition of the polar region; different studies have used different equatorward boundaries. Given that in the Southern Hemisphere (SH) the sea ice extends considerably farther equatorward than 75°S, we chose to define the NH and SH polar regions symmetrically as 60°– 90°N, and 60°–90°S, respectively (hence our choice of regressions in these regions). Some of the feedbacks have the effect of warming quite uniformly, whereas others cool in some places and warm in others, so only comparing the equilibrium partial temperature responses in the polar region does not give a full understanding of contributions to polar amplification. Therefore, we use the normalized difference in the warming between polar and tropical regions for each partial temperature contribution, determined from the regressions in these regions, so that the NH and SH partial polar amplifications are defined respectively as

TABLE 1. 2 × CO_2 experiments equilibrium temperature response and polar amplification.

Model	Global mean ΔT at equilibrium (K)	Annual mean NH polar amplification [Eq. (13)]	Annual mean SH polar amplification [Eq. (14)]
GISS ER	2.72	0.52	0.11
NCAR CCSM3.0	2.74	0.71	0.87
GFDL CM2.0	2.94	0.85	0.38
CSIRO Mk3.0	3.08	0.66	0.54
MRI CGCM2.3.2a	3.22	0.45	0.78
CCCma CGCM3.1 (T47)	3.65	0.83	0.93
MIROC 3.2 (medium res.)	4.00	1.05	0.65
UKMO HadGEM1	4.45	1.07	0.72
Multimodel mean	3.35	0.80	0.64

$$\mathrm{Amp}_{\mathrm{NH},i} = \frac{\Delta T_{i,60\mathrm{N}-90\mathrm{N}} - \Delta T_{i,30\mathrm{N}-30\mathrm{S}}}{\overline{\Delta T}} \quad \text{and} \quad (13)$$

$$\mathrm{Amp}_{\mathrm{SH},i} = \frac{\Delta T_{i,60\mathrm{S}-90\mathrm{S}} - \Delta T_{i,30\mathrm{N}-30\mathrm{S}}}{\overline{\Delta T}}. \quad (14)$$

This means when there is no partial polar amplification our metric will be zero.

3. Model data

a. 2 × CO_2 experiments

The eight slab ocean models from the CMIP3 multimodel dataset with results available for the whole of the integration from 2 × CO_2 experiments were chosen. These models have equilibrium surface temperature changes across most of the range given in Meehl et al. (2007) (see Table 1). The differences in seasonal and annual mean TOA radiative flux components and surface temperature data compared to those in the equivalent control run were determined at each grid box. The methods for determining local feedback parameters, equilibrium partial temperature responses, and contributions to polar amplification as described in section 2 were applied.

b. HadSM3 experiments

N. Stuber et al. (2011, manuscript in preparation) carried out a number of idealized aerosol perturbation experiments as well as 2 × CO_2 and +2% solar constant experiments using HadSM3 to investigate mechanisms of tropospheric adjustment. HadSM3 (Williams et al. 2001), the slab ocean configuration of the Hadley Centre Unified Model (v.4.5), includes the direct and semidirect effects of aerosols but not the indirect effects. A globally homogeneous layer of either purely scattering (single scattering albedo = 1) or partially absorbing aerosol was introduced at one of low-cloud level (LC), middle-cloud level (MC), high-cloud level (HC), or a tropopause-following level (UT). For the absorbing aerosol they chose a single scattering albedo of 0.75 to result in warming for the LC case. The mixture of aerosols in the real world has been estimated to have a single scattering albedo of 0.8–0.96 (Hansen et al. 1997). Their study showed that the surface temperature response to a purely scattering aerosol perturbation is largely independent of the height at which the perturbation is applied, but for absorbing aerosol the response is strongly dependent on the height of the perturbation, with some cases giving surface warming and others giving surface cooling in agreement with Hansen et al. (1997). The climate was less sensitive to scattering aerosol than CO_2 at all altitudes regardless of whether the standard instantaneous/stratosphere-adjusted forcing or the regression troposphere-adjusted forcing was used. For absorbing aerosol it was not possible to predict the sign of the temperature response using the standard forcing and the climate sensitivity parameter determined from the regression forcing was greater than that for 2 × CO_2 for all perturbation heights except for the MC case.

We took the radiative flux and surface air temperature outputs of these 2 × CO_2, +2% solar constant, HC absorbing aerosol (HCabs), and LC scattering aerosol (LCscat) experiments. Although not realistic, these two aerosol experiments were chosen as they give a good range of climate sensitivity parameters and radiative forcing even after allowing for tropospheric adjustments (see Table 3) and therefore will provide a good test of how constant the pattern of feedbacks are under different forcing patterns. Despite the aerosol perturbation being applied homogeneously across the world, both the instantaneous forcing and troposphere-adjusted forcing were far from homogeneous. The methods for determining local feedback parameters, equilibrium partial temperature responses, and contributions to polar amplification using the regression forcing as described in section 2 were applied. In the case of the Planck feedback, we did not have access to the three-dimensional specific humidity and temperature fields and therefore used the CMIP3 multimodel mean for all HadSM3

forcing mechanisms. The intermodel differences in CMIP3 Planck feedback are very small and therefore we believe that using a model-specific Planck feedback parameter would make little difference to our results.

4. Results

a. How well does the linear model of feedback fit?

The goodness of fit was determined using an F test from the linear regressions. In the global mean, the linear model of feedback generally fits very well for all components (p value ≈ 1), agreeing with previous work (e.g., Gregory and Webb 2008). However, for one CMIP3 model in the annual mean and a few models in different seasons the longwave and/or shortwave cloud global mean regressions gave a p value as low as 0.2. In these cases, the feedback parameter was very small so there is virtually no correlation between radiative flux change and surface temperature change. The regressions in the polar regions and tropics generally gave good linear fits in the annual mean but in some seasons for some models the tropical shortwave cloud feedback gave a poor linear fit (p value < 0.1). As with the global mean, this again was due to the feedback being very small. When the p value becomes less than 0.1 this may suggest the linear analysis becomes seriously questionable. However, the error in the feedback in these cases is not large. Where we show results from these regressions we also show the associated errors, where possible, which we believe give a better indication of the appropriateness of the linear model. In the zonal mean, we again found for all feedbacks in all seasons and the annual mean the p value dropped to $\sim$0.1 when the feedback parameter was very small, that is, crosses the zero line. This happens more often for cloud feedbacks. It also happens for a few models in some seasons for water vapor plus lapse rate feedback near the equator when the water vapor plus lapse rate and Planck feedbacks completely oppose each other, although generally the longwave clear-sky regressions are very good. The regressions on the multimodel mean of the radiative flux and temperature changes were generally better in all seasons than those for individual models because taking a mean of multiple simulations averages out some noise. The standard deviations obtained from the regressions are still small compared to the variations in the feedback parameter across the latitudes, and thus we believe the overall patterns of feedback are robust. We looked at a random sample of the residuals plotted against the expected ΔRs and mostly found these residuals were evenly distributed suggesting our linear model is appropriate. Only in three cases [for albedo feedback around 60°S for the Commonwealth Scientific and Industrial Research Organisation mark 3.0 (CSIRO Mk3.0), Met Office (UKMO) Hadley Centre Global Environmental Model version 1 (HadGEM1), and the Model for Interdisciplinary Research on Climate 3.2, medium-resolution version (MIROC 3.2{medres})] was there any suggestion of nonlinearity. In these cases, the albedo feedback is reducing slightly as the temperature increases. This also has the effect of giving a nonzero intercept, which we do not expect for the Winton shortwave albedo regressions. Figure 1 shows the annual mean zonal mean regressions for the UKMO HadGEM1 model (good linear fits) and the Meteorological Research Institute Coupled General Circulation Model, version 2.3.2a (MRI CGCM2.3.2a) model (worst linear fits) at 60°S (one of the best locations for linear fit) and 30°N (one of the worst locations for linear fit). Performing the regressions in each $10° \times 10°$ grid box gave poor linear fits (p value < 0.2) in many locations for the surface albedo, shortwave cloud and longwave cloudy-sky components, and over a few tropical locations for the longwave clear-sky component. Given these results we suggest our linear analysis is not applicable to $10° \times 10°$ grid boxes but is applicable to zonal means. We therefore concentrate our discussions on results from zonal mean regressions and from polar and tropical regressions, and we only discuss the features where linear fit is good.

b. Comparison between different forcing definitions

The annual mean forcing determined by regression and the archived stratosphere-adjusted forcing, where available, are shown for each model in Fig. 2. The regression forcing follows a similar pattern to the stratosphere-adjusted forcing, being positive everywhere with a maximum near the equator and minima at the poles. The stratosphere-adjusted forcing is mostly within plus/minus two standard deviations of the regression forcing, but we would expect differences owing to rapid tropospheric adjustments. The feedback parameters and the equilibrium partial temperature changes for the $2 \times CO2$ CMIP3 experiments, as calculated from the stratosphere-adjusted forcing (where available) and the mean equilibrium radiative flux and surface temperature changes, showed a similar zonal mean pattern to those calculated by regression. The differences between the two methods are significant in a small number of latitudes, particularly for the cloud-related components, but the feedback parameters and equilibrium partial temperature changes from the stratosphere-adjusted forcing are generally within plus/minus two standard deviations of those calculated using F_{regr} (not shown). Our global mean regressions give very similar results to those of Gregory and Webb (2008) and Andrews and Forster (2008), who show there

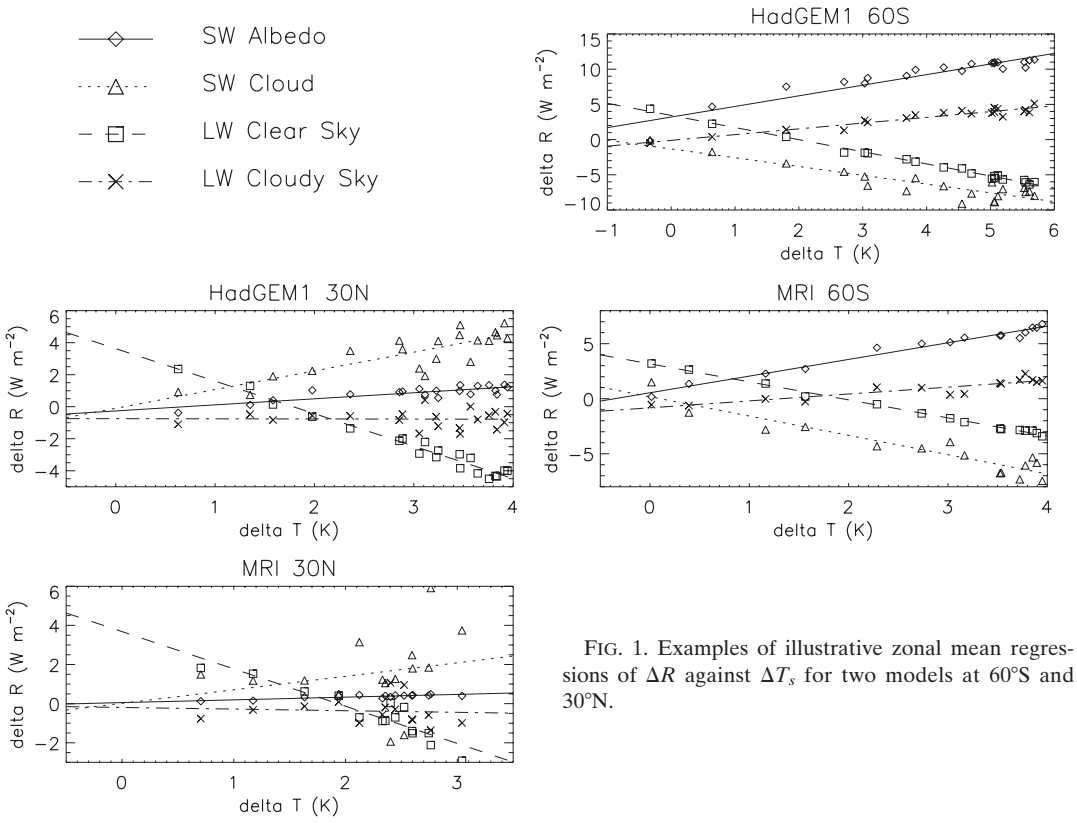

FIG. 1. Examples of illustrative zonal mean regressions of ΔR against ΔT_s for two models at 60°S and 30°N.

is a small but significant tropospheric adjustment in the global mean forcing for CO_2. Small differences between the methods in the zonal mean may add up to more significant differences in the global mean (note that errors in the zonal means are greater than in the global mean). Many studies have shown that for aerosols, the difference between the instantaneous/stratosphere-adjusted and troposphere-adjusted forcing is considerable and argue that the rapid tropospheric adjustments should be included within the forcing rather than the feedback, making the climate sensitivity parameter closer to that for $2 \times CO_2$ (Hansen et al. 1997, 2005; Shine et al. 2003; Lohmann et al. 2010). Our own work supports this in that the zonal mean pattern of feedback parameters for the HadSM3 HCabs experiment, as calculated from the instantaneous forcing, was unphysical (e.g., longwave feedback calculated from the instantaneous forcing has values of around -100 W m^{-2} K^{-1} in some latitudes, not shown). Therefore, only the results from the regression method are discussed further.

c. *Patterns of feedback from 2 × CO_2 experiments*

Figure 3 shows the shortwave clear-sky feedback, shortwave cloudy-sky (CRF) feedback, surface albedo (Winton) feedback, and shortwave cloud (Winton) feedback for the National Center for Atmospheric Research (NCAR) Community Climate System Model, version 3 (CCSM3.0) model for annual means. We also show the plus/minus two standard deviation in the feedbacks from the regressions to show the typical errors in our zonal mean feedbacks. This figure shows that clouds provide masking of the surface albedo feedback in the cryosphere regions reducing its strength to about half that of the shortwave clear-sky feedback. This is true of all seasons and typical of all the models analyzed, although the strength of the masking does vary to some extent. Note that Qu and Hall (2006) determined that changes in planetary albedo are about half the change in surface albedo and that this fraction did not vary considerably between the 17 models analyzed. The shortwave CRF feedbacks and the Winton feedbacks behave very similarly in tropical regions showing that cloud masking has little effect on this region.

The feedback parameters from the zonal mean regressions for annual means and all models are shown in Fig. 4, and feedback parameters for the multimodel mean zonal mean regressions for seasonal means are shown in Fig. 5. The multimodel mean feedback patterns show seasonal behavior typical of most models.

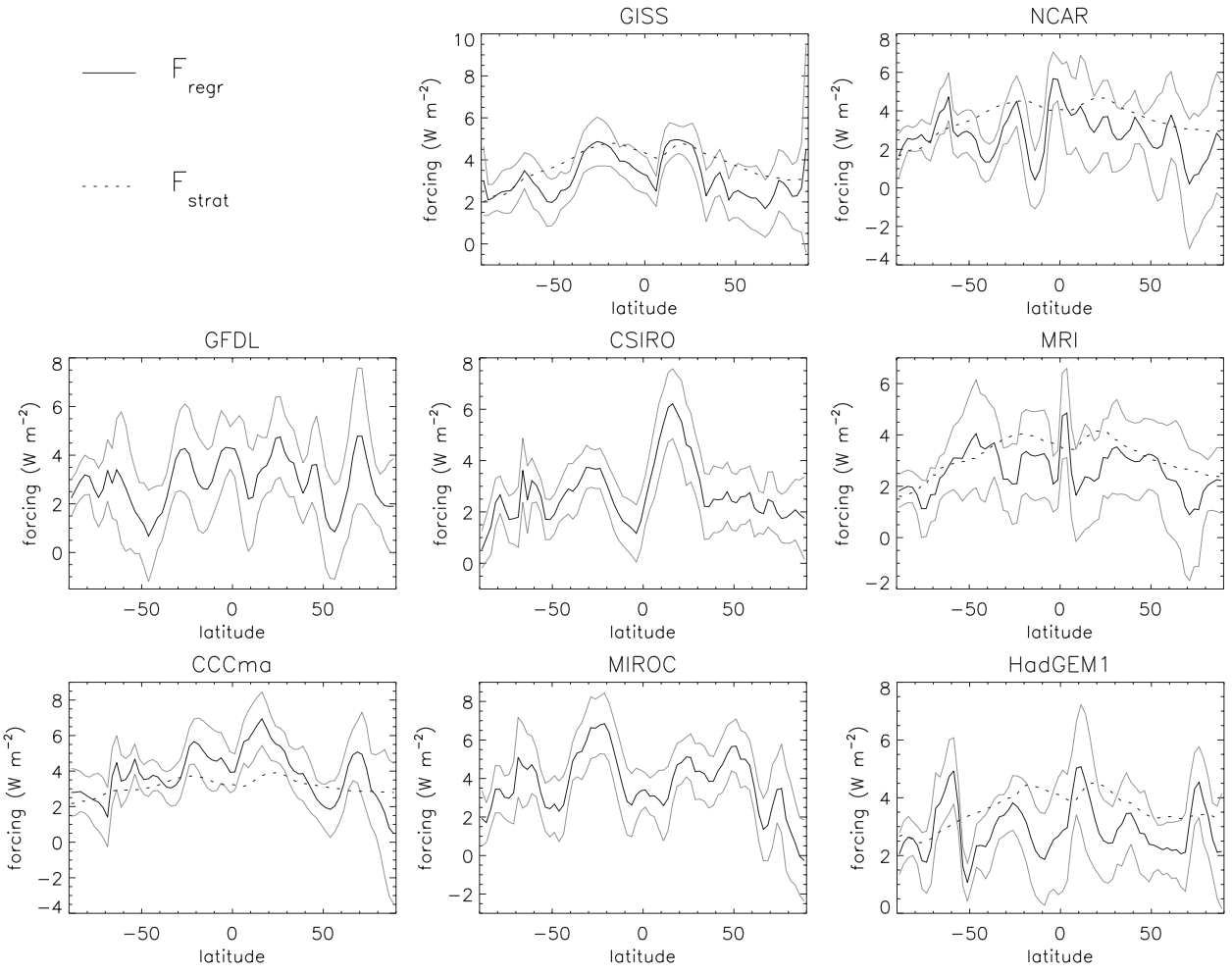

FIG. 2. Annual mean, zonal mean forcing for CMIP3 models. The solid black lines show the forcing determined from regression and the dotted lines show the archived stratosphere-adjusted forcing where available. The gray lines show $\pm 2\sigma$ for the regression forcing.

The Planck feedback (Figs. 4a and 5a) is negative everywhere and is the most uniform feedback across latitudes, but it is slightly more negative in the tropics owing to its higher temperatures. It varies seasonally more in higher latitudes where there is greater seasonal variation in temperature.

The shortwave feedbacks obviously have no effect poleward of about 65° during the winter when sunlight is absent. The SH sea ice zone shows very strong positive surface albedo feedback in the SH spring and summer and a much less positive surface albedo feedback in the SH autumn and winter (Fig. 5b). This peak tends to move poleward through the SH spring and summer, following the northern edge of the sea ice as it retreats poleward and more solar radiation reaches higher latitudes. The greatest variation between models in the location of this peak (up to 5°) occurs in the SH spring, whereas the greatest variation in the height (strength of the feedback) of this peak (up to 12 W m^{-2} K^{-1}) occurs in the SH summer (not shown). The surface albedo feedback poleward of 80°S is very small in all seasons. From 50°S to 25°N there is essentially no surface albedo feedback in any season.

In the NH there is positive surface albedo feedback in the annual mean from 25° to 90°N. This positive feedback is constrained to 25°–55°N in the NH winter owing to the absence of sunlight in high latitudes. The peak centered on 33°N (Fig. 4b) is due to the Himalaya. In the NH spring the greatest surface albedo feedback is from 45° to 75°N mainly because of snow over land, whereas during the NH summer the peak narrows and moves poleward. Snow over land has largely melted by the summer but the sea ice melts later in the year. There is very little surface albedo feedback in the NH autumn when snow and ice coverage is small. The eight models behave very differently in the NH summer poleward of 80°N (differences

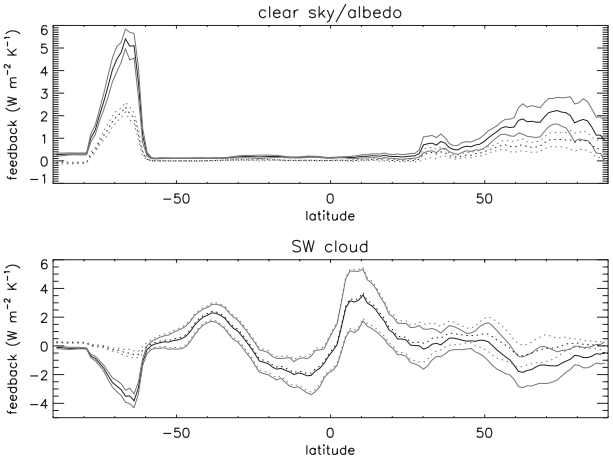

FIG. 3. Annual mean, zonal mean shortwave feedback parameters for the NCAR CCSM3.0 model forced with $2 \times CO_2$. The solid line uses the CRF method, and the dotted line uses the Winton (2006a) method. The gray lines indicate $\pm 2\sigma$.

>10 W m^{-2} K^{-1}) where three models have a surface albedo feedback that becomes negative (not shown). For most of these models the error in the feedback at these high latitudes during summer is quite large and, therefore, these results should be interpreted with caution. The Goddard Institute for Space Studies Model E-R (GISS-ER) behaves quite differently to other models in having the weakest annual mean surface albedo feedback in the SH sea ice zone but the strongest annual mean surface albedo feedback in the Himalaya (Fig. 4b). This weak annual mean surface albedo feedback in the SH sea ice zone contributes to it having one of the smaller equilibrium temperature changes and a small SH polar amplification (see Table 1).

The shortwave cloud (Winton) feedback (Figs. 4c and 5c) generally shows strong negative feedback collocated with the positive surface albedo feedback. Low cloud tends to increase where sea ice melts leading to the anticorrelation between surface albedo and shortwave cloud feedback. However, the strength of this anticorrelation varies with models, and for the Canadian Centre for Climate Modelling and Analysis (CCCma) Coupled General Circulation Model, version 3.1 (CGCM3.1) (T47) there is no correlation at all (Fig. 4c). In low and mid latitudes there is considerable difference (up to 4–7 W m^{-2} K^{-1} depending on the season) between models in shortwave cloud (Winton) feedback (not shown), although the errors in the feedback may be up to ± 2 W m^{-2} K^{-1} here. This is also true for the longwave cloudy sky feedback (differences up to 5 W m^{-2} K^{-1}) (not shown). The longwave cloudy-sky feedback (Figs. 4e and 5e) tends to be anticorrelated with the shortwave cloud (Winton) feedback,

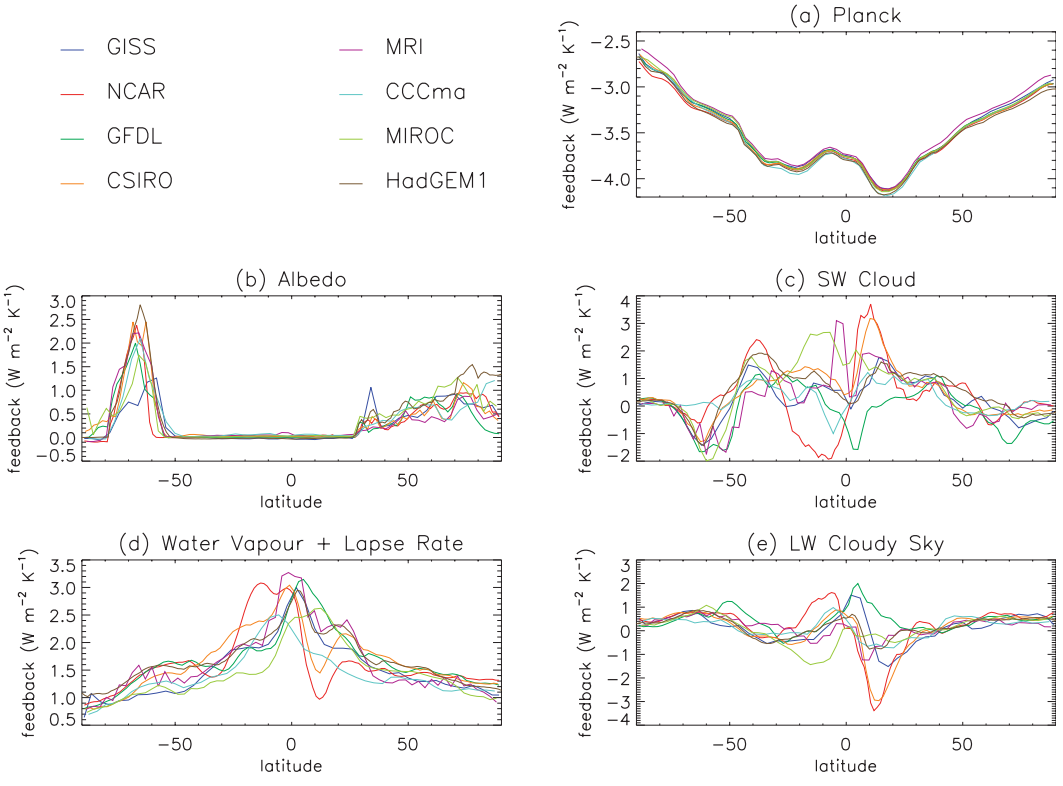

FIG. 4. Annual mean, zonal mean feedback parameters for the different models forced with $2 \times CO_2$.

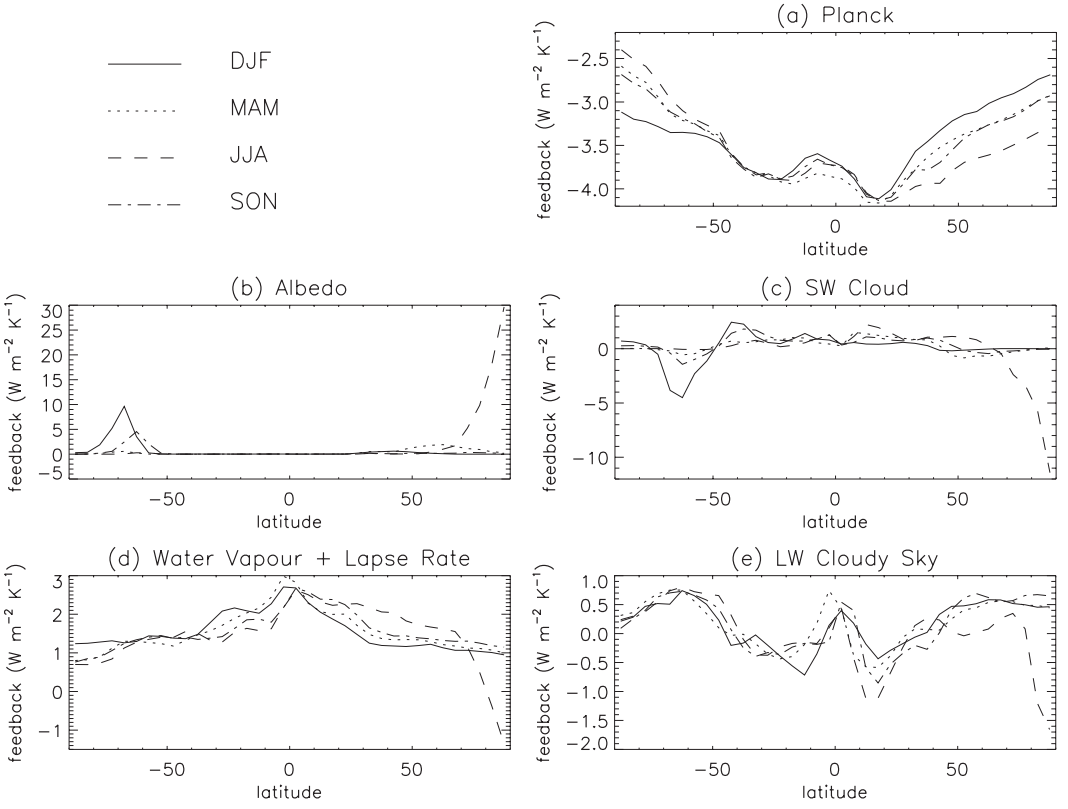

FIG. 5. 2 × CO_2 experiments multimodel mean, zonal mean feedback parameters for each season.

although this is much clearer in spring and autumn and is not the case in high NH latitudes in summer. More cloud in general would lead to more shortwave reflection (negative feedback) but more trapping of longwave radiation (positive feedback).

The water vapor plus lapse rate feedback (Figs. 4d and 5d) is generally positive everywhere and tends to be higher in the tropics. However, negative water vapor plus lapse rate feedback is found in summer for MIROC 3.2 and UKMO HadGEM1 around 80°N (not shown) and for the multimodel mean poleward of 80°N, but note that the errors are quite large here. In the tropics, there is more intermodel spread (up to 2 W m^{-2} K^{-1}) (not shown). It should be noted that, unlike our shortwave analysis, our methodology cannot evaluate cloud-masking effects in the longwave; if these had been taken into account this feedback strength would have been reduced (Soden et al. 2008). The lapse rate feedback has been shown to be negative in the tropics and positive at high latitudes (Bony et al. 2006) suggesting that the feedback due to water vapor alone must be particularly high in the tropics. The clear tropical pattern in the NCAR CCSM3.0 model with significantly different feedback strength in each hemisphere is seen in the water vapor plus lapse rate feedback and both cloud feedbacks (Fig. 4). It is likely that water vapor and cloud amount are positively correlated (Soden et al. 2008).

d. *Equilibrium partial temperature changes from 2 × CO_2 experiments*

Not surprisingly, the patterns of equilibrium partial temperature changes for the different feedbacks are similar to the patterns of feedbacks themselves, but high-latitude temperatures are enhanced because the magnitude of the Planck feedback is less at high latitudes [note we are dividing by the Planck feedback to obtain the temperature change, Eq. (12)] and the temperature change required to balance the forcing is therefore greater at high latitudes (Joshi et al. 2003). Also the temperature response due to each feedback is affected by the strength of other feedbacks.

The surface albedo feedback gives a positive temperature change that is greatest in high latitudes in spring and summer (Fig. 6a). The spread of surface albedo feedback equilibrium partial temperature changes between the different models is also greatest for these seasons (up to 12 K for the SH sea ice zone and ~5 K for the NH polar region) (not shown).

The shortwave cloud (Winton) feedback tends to cool the high latitudes and warm the low latitudes with the

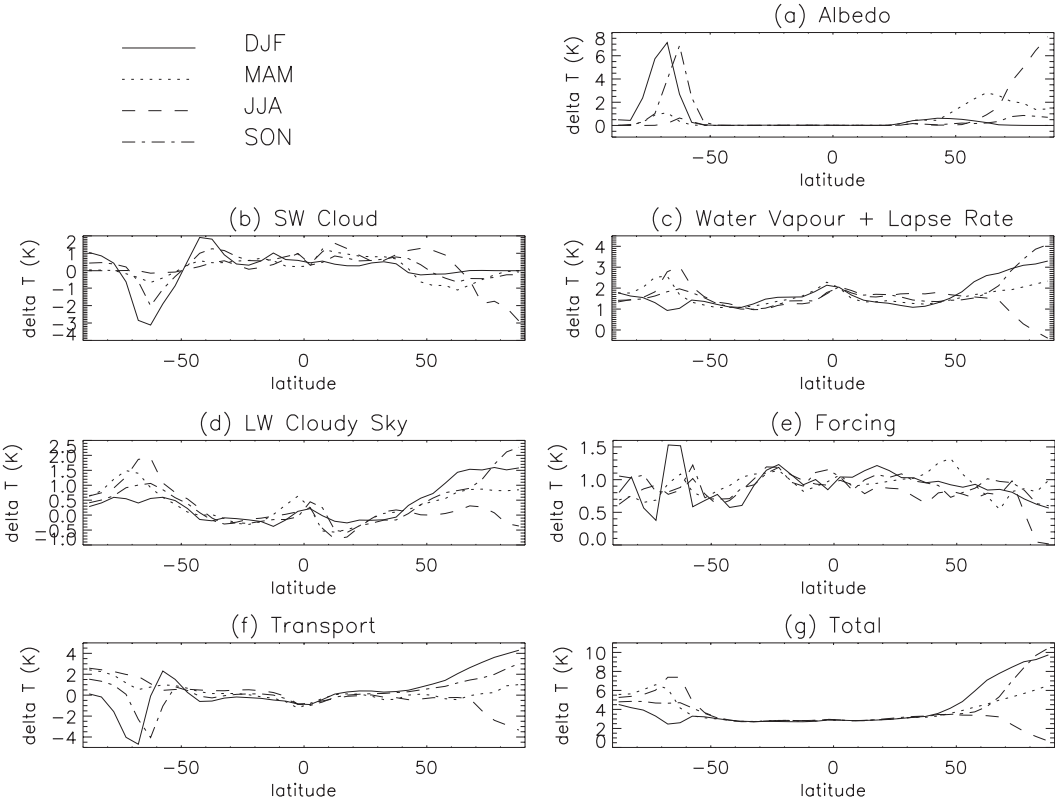

FIG. 6. 2 × CO_2 experiments multimodel mean, zonal mean equilibrium partial temperature changes for each season.

greatest high-latitude cooling occurring in the spring and summer (Fig. 6b). There is a large intermodel spread of shortwave cloud (Winton) equilibrium partial temperature changes in the tropics in all seasons (~4 K) and in high latitudes in summer (~7 K) (not shown).

The water vapor plus lapse rate feedback tends to warm the NH mid- to high latitudes and the SH sea ice zone most in autumn and winter (Fig. 6c). The intermodel spread in the polar regions in these seasons is ~3 K (not shown). Given that this feedback has not been adjusted for the masking effect of clouds in the longwave, the water vapor plus lapse rate feedback equilibrium partial temperature change would likely be less positive than shown.

The longwave cloudy-sky feedback tends to warm the mid-to-high latitudes, particularly in autumn and winter (Fig. 6d). The tropics show greatest spread between models (~3 K) for the longwave cloudy-sky equilibrium partial temperature change (not shown). With cloud-masking effects removed, it is likely that the equilibrium partial temperature change due to longwave cloud effects would be more positive than shown.

The equilibrium partial temperature change due to the forcing is generally more uniform across latitudes (Fig. 6e) but there is a spread of up to 2 K between models (not shown). Errors in the equilibrium partial temperature change due to the forcing, shortwave cloud, and longwave cloudy-sky feedbacks can be up to 1 K (not shown).

In the annual mean when our transport term just includes meridional heat transport, it can be seen that there is decreased transport of heat into the SH sea ice zone, counteracting the strongly positive sea ice albedo feedback (Fig. 6f). In the SH spring and summer when the albedo feedback is strongest, our transport term, which also includes the seasonal heat storage term, is particularly negative in the SH sea ice zone. The same effect can also be seen in the NH summer. In both hemispheres in autumn and winter, the transport term generally warms the high latitudes. The largest spread in the temperature change due to our transport term between models occurs in the high-latitude summers (up to 10 K in the SH and 8 K in the NH) (not shown). Further analysis is required to separate the contributions from heat storage and heat transport in the different seasons. Lu and Cai (2009a) find longwave CRF and ocean heat release contribute positively to the seasonal pattern of high-latitude warming, but these are secondary to the

TABLE 2. $2 \times CO_2$ experiments annual mean, global mean equilibrium partial temperature changes and polar amplifications. Here, a = mean of all models, and b = multimodel mean regression result.

Partial temperature		Global mean $\Delta T \pm 2\sigma$ (K)	NH partial polar amp [Eq. (13)] as % of total $\pm 2\sigma$	SH partial polar amp [Eq. (14)] as % of total $\pm 2\sigma$
Surface albedo	a	0.35 ± 0.26	55.7 ± 23.7	115.3 ± 94.0
	b	0.35 ± 0.01	54.6 ± 2.8	100.9 ± 3.3
Shortwave cloud	a	0.40 ± 0.48	−50.8 ± 52.5	−92.8 ± 194.1
	b	0.36 ± 0.03	−45.9 ± 5.5	−62.4 ± 4.0
Water vapor plus lapse rate	a	1.57 ± 0.57	19.2 ± 27.3	−9.2 ± 134.1
	b	1.56 ± 0.01	22.8 ± 2.0	17.1 ± 2.8
Longwave cloudy sky	a	0.12 ± 0.23	41.9 ± 32.2	72.7 ± 129.7
	b	0.12 ± 0.02	39.8 ± 2.5	55.2 ± 2.9
Forcing	a	0.91 ± 0.30	−9.5 ± 19.0	−5.6 ± 38.0
	b	0.95 ± 0.02	−6.9 ± 7.1	−3.2 ± 7.4
Transport	a	0.01 ± 0.12	43.5 ± 61.9	19.6 ± 153.7
	b	0.01	35.7	−6.7

contribution from their clear-sky downward longwave component. They use the surface energy budget to perform their calculations and therefore do not separate the components in the same way as us; their clear-sky downward longwave component includes poleward sensible and latent heat transport and the forcing as well as water vapor feedback, and their vertical latent and sensible heat fluxes (manifested as lapse rate feedback and included with our water vapor feedback) and ocean heat storage (included with our transport term) are separated.

The global mean annual mean equilibrium partial temperature changes were calculated from the zonal mean regression results. We use the zonal mean regression results so that the transport term is not lost in the other terms, which would be the case if we used the global mean regression results (ΔR goes to zero in the annual global mean at equilibrium). However, the results are not very different from the global mean regression results. The ensemble mean of these equilibrium partial temperature changes for all the models plus/minus two standard deviations and the multimodel mean equilibrium partial temperature changes plus/minus two standard deviations are shown in Table 2. We find the water vapor plus lapse rate feedback contributes most to the intermodel spread of equilibrium partial temperature change. The shortwave cloud (Winton) feedback gives the second greatest intermodel spread. This contrasts with Dufresne and Bony (2008) who find the temperature contribution from cloud feedback contributed considerably more intermodel spread than any other feedback. Differences may be partly accounted for as they used a stratosphere-adjusted forcing and performed their calculations with coupled atmosphere–ocean models. Andrews and Forster (2008) also found that use of the regression forcing rather than the stratosphere-adjusted forcing reduced the intermodel spread of cloud feedback. We find that the equilibrium partial temperature change due to the forcing gives the third greatest contribution to intermodel spread.

e. *Polar amplification contributions from $2 \times CO_2$ experiments*

Both the NH and SH show the greatest warming during their respective winters and the least warming during their respective summers, whereas the tropics show little variation throughout the seasons (Fig. 6). The partial polar amplifications for all models in each season and the annual mean are shown in Figs. 7 and 8 for the NH and SH, respectively. We also include the error (plus/minus two standard deviations) for each partial polar amplification. In all seasons, the transport term consists of contributions from horizontal heat transport and heat storage.

In summer, there is virtually no polar amplification especially in the NH despite there being a large warming due to the surface albedo feedback. This is counteracted largely by high-latitude cooling due to the transport term and/or shortwave cloud (Winton) feedback. Lu and Cai (2009a) also find the large contribution from surface albedo feedback is counteracted by negative CRF in the shortwave. For some models, the water vapor feedback and/or forcing also warm the tropics considerably more than the polar region.

In autumn and winter, the main positive contributors to both the NH and SH polar amplification are the transport term, followed by longwave cloudy-sky feedback. For some models, the water vapor plus lapse rate feedback also has a non negligible contribution.

In spring, the main positive contributors to the both the NH and SH polar amplification are the surface albedo feedback, followed by longwave cloudy-sky feedback, although some models in the NH have a noteworthy contribution from the transport term and water vapor plus lapse rate feedback.

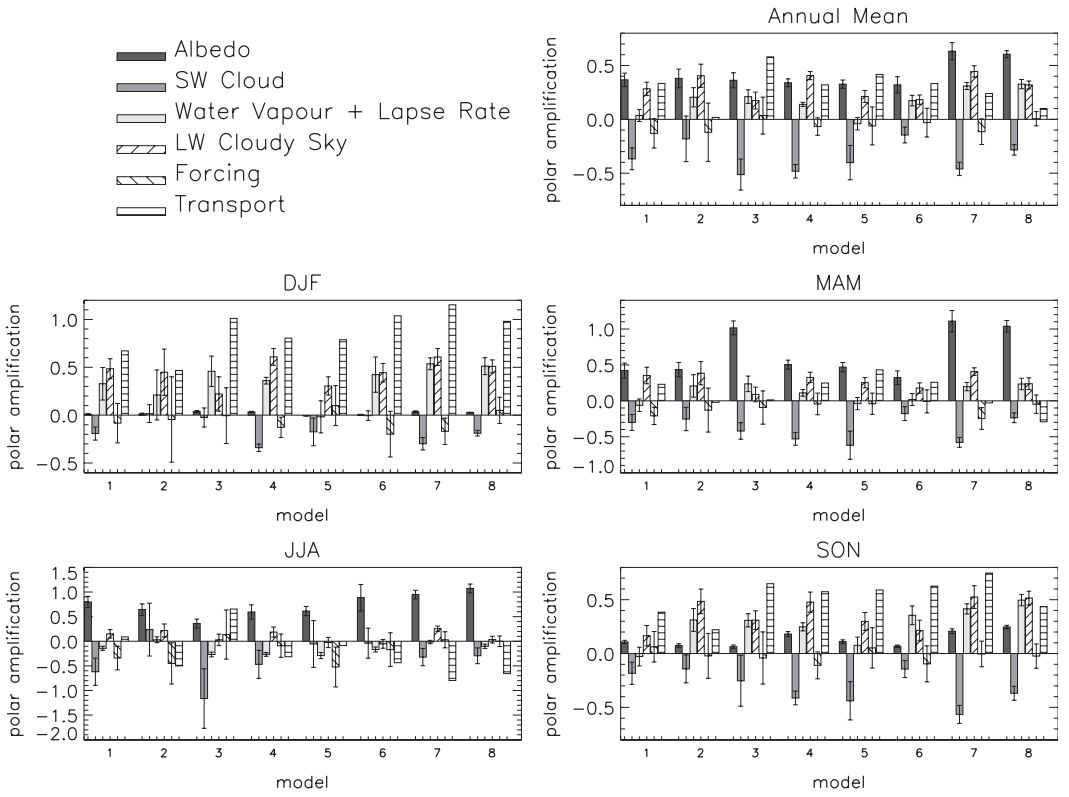

FIG. 7. NH partial polar amplifications [Eq. (13)] for each model forced with $2 \times CO_2$ for the annual mean and the different seasons. Model numbers are given in Table 1.

In all seasons, the shortwave cloud (Winton) feedback gives a negative contribution for all models except for NCAR CCSM3.0, which has a positive contribution to the NH polar amplification, and CCCma CGCM3.1 (T47), which has a positive contribution to the SH polar amplification in their respective summers. For NCAR CCSM3.0 the partial temperature change due to shortwave cloud (Winton) feedback in summer is negative above 80°N but positive between 60° and 80°N (not shown), giving an overall positive contribution to the NH polar amplification. The anticorrelation between albedo and shortwave cloud feedback is strongest where sea ice melts and other factors may play an important part in shortwave cloud feedback over NH high-latitude land. It should be noted that the error in the shortwave cloud feedback partial polar amplification for the NCAR CCSM3.0 model is large, suggesting that this partial polar amplification could actually be negative. As mentioned earlier, CCCma CGCM3.1 (T47) is unusual in not showing the anticorrelation between surface albedo and shortwave cloud feedbacks in the SH sea ice zone. Further analysis would be required to understand why this might be.

The ensemble mean of the annual mean partial polar amplifications as percentages of the total polar amplification are given in Table 2. We also give the annual mean partial polar amplifications as percentages of the total polar amplification for the multi–model mean regression results. These data indicate that the surface albedo feedback gives the greatest contribution in both hemispheres in the annual mean. In the NH the next greatest contribution comes almost equally from the horizontal heat transport and longwave cloudy sky feedback, followed by the contribution from the water vapor plus lapse rate feedback. In the SH the next greatest contribution comes from the longwave cloudy sky feedback. Horizontal heat transport and water vapor plus lapse rate feedback give the next greatest contributions. We find there is generally more intermodel spread in the annual mean SH polar amplification, but in both hemispheres this spread comes mostly from the contributions from horizontal heat transport and shortwave cloud (Winton) feedback.

f. Patterns of forcing and feedback from HadSM3 experiments

Both the zonal mean instantaneous and regression forcings were found to be highly inhomogeneous for the HCabs experiment despite a homogeneous aerosol

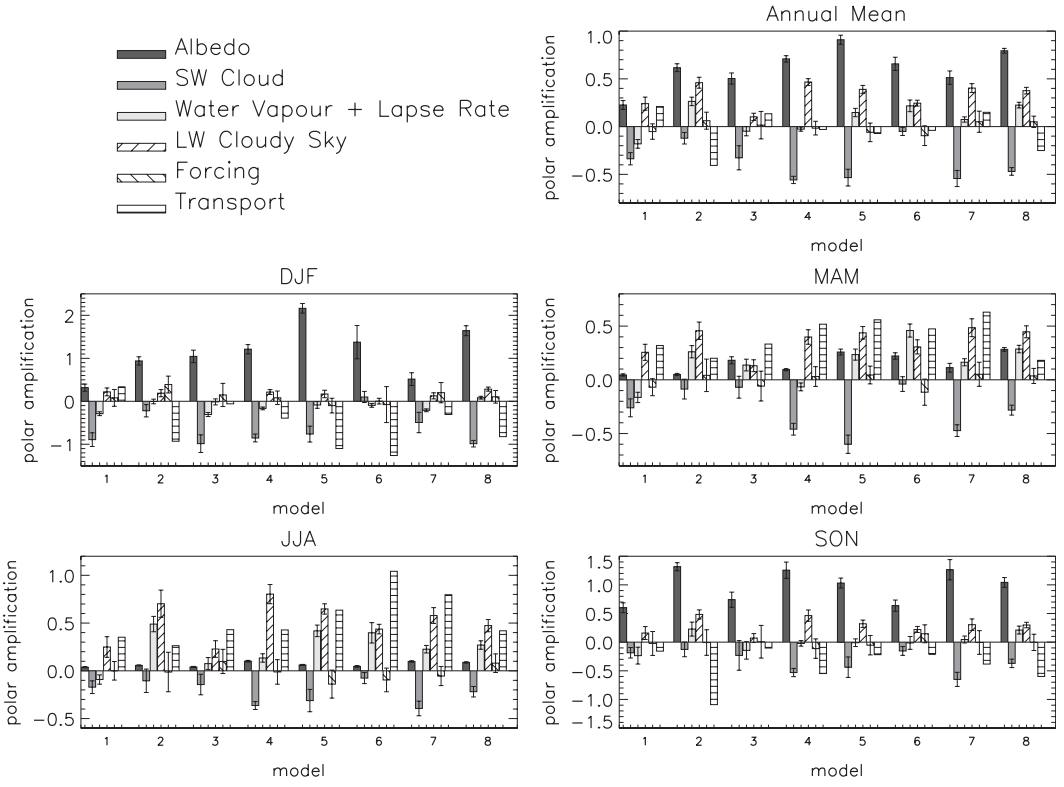

FIG. 8. SH partial polar amplifications [Eq. (14)] for each model forced with $2 \times CO_2$ for the annual mean and the different seasons. Model numbers are given in Table 1.

change (Fig. 9a). The zonal mean regression forcing was found to be more inhomogeneous and considerably reduced compared to the instantaneous forcing resulting in positive forcing in high latitudes and negative forcing in the tropics. Rapid adjustments in clouds, lapse rate, and water vapor mixing ratio cause the difference between the regression and instantaneous radiative forcings. Details of these changes are described more fully in N. Stuber et al. (2011, manuscript in preparation). We find our regression forcing is virtually identical to the instantaneous forcing in the shortwave clear-sky component, but the other three components show large differences particularly in the cloudy sky components (Figs. 9b, 9c, 9d, and 9e).

The high cloud was found to decrease immediately whereas the low and mid cloud increase a little immediately and then increase further throughout the integration. The initial cloud changes result in reducing the shortwave and longwave cloudy-sky forcings (Figs. 9c and 9e). The further increases in mid and low cloud combine to form the total cloud feedback.

The equilibrium temperature profile response shows a decrease in the lapse rate that is particularly strong in the high latitudes (not shown). In the global mean, this lapse rate decrease is already manifested after two years. This would give a negative forcing in the global mean. The water vapor mixing ratio initially increases in the troposphere (positive forcing) but in the stratosphere it decreases in the tropics (negative forcing) and increases in the high latitudes (positive forcing). The combined effects of lapse rate and water vapor adjustments give rise to the longwave clear-sky component of the regression forcing (Fig. 9d). Throughout the integration there is a further decrease in stratospheric water vapor in the tropics, which would contribute positively to the tropical water vapor plus lapse rate feedback.

The feedbacks from regression show similar patterns for all forcing mechanisms, but the $2 \times CO_2$ and +2% solar forcing have the most similar patterns (not shown). The surface albedo feedback appears stronger for aerosol forcing than $2 \times CO_2$ and +2% solar forcing particularly in the SH and also extends closer to the equator in the SH owing to the ice edge being closer to the equator in the colder temperatures of the aerosol-forced simulations. This can also be seen in the temperature response due to the surface albedo feedback (Fig. 10a). The shortwave cloud (Winton) feedback has a more variable pattern for aerosol forcing in the tropics and is generally more positive for the HCabs experiment and less positive for the LCscat

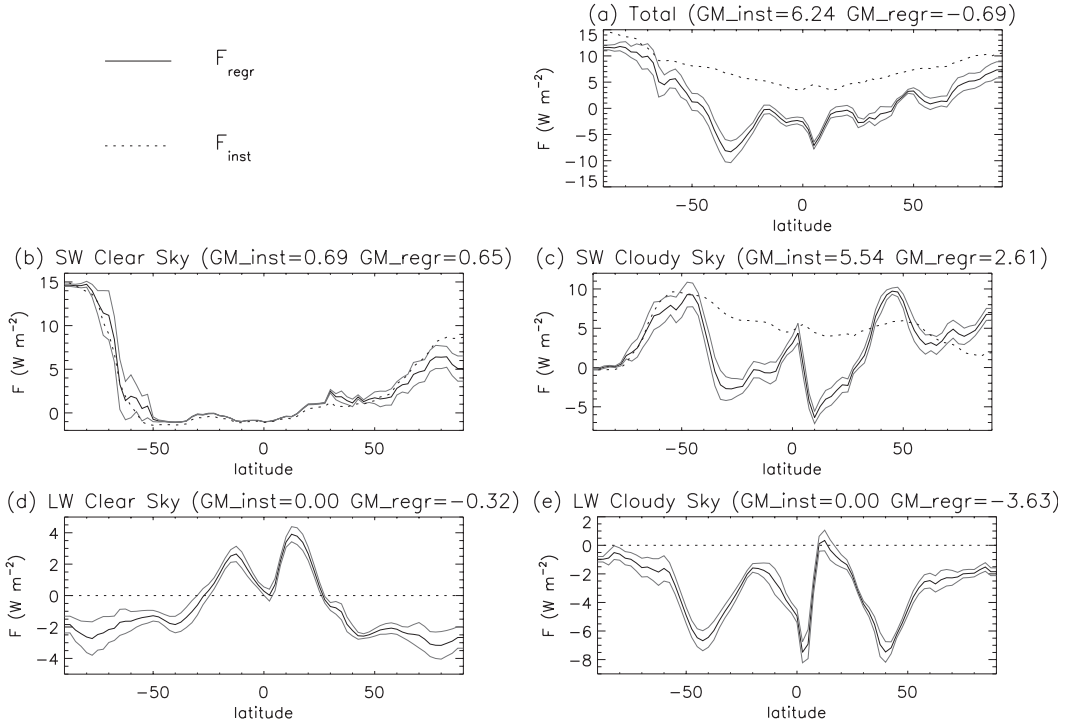

FIG. 9. Annual mean, zonal mean instantaneous and regression forcing for HadSM3 HCabs experiment. The gray lines show $\pm 2\sigma$ for the regression forcing.

experiment than $2 \times CO_2$ and +2% solar experiments (not shown). The water vapor plus lapse rate feedback and the longwave cloudy-sky feedback show the greatest variation between forcing mechanisms in the tropics. The longwave cloudy-sky feedback is also greater for both aerosol experiments than $2 \times CO_2$ and +2% solar experiments in the SH sea ice zone and this is apparent in the temperature response (Fig. 10d).

g. *Equilibrium partial temperature changes from HadSM3 experiments*

Equilibrium partial temperature changes for the HadSM3 experiments are shown in Fig. 10. Given that the forcing patterns are different for each experiment we would not expect the temperature changes to be the same. However, the equilibrium temperature response pattern in the HCabs experiment does not match the regression forcing pattern in anyway, with cooling happening almost everywhere and the greatest cooling occurring in high latitudes (Figs. 10e and 10g) where the forcing is strongly positive. The equilibrium partial temperature change due to the horizontal heat transport (Fig. 10f) shows strongly reduced poleward heat transport in the HCabs experiment that counteracts the forcing (Fig. 10e). Given that the zonal mean temperature is cooling throughout the integration, this implies the change in horizontal heat transport is manifested early. Analysis found that the Hadley circulation was slowed down causing the rapid decrease of stratospheric water vapor in the tropics.

The global mean equilibrium partial temperature change determined from the zonal means divided by the global mean regression forcing gives a measure of the contribution to the global mean climate sensitivity parameter (Fig. 11). The HCabs experiment has a higher climate sensitivity parameter owing to the water vapor plus lapse rate feedback but also because of the surface albedo feedback, the horizontal heat transport, and the longwave cloudy sky feedback. The LCscat experiment has a lower climate sensitivity parameter because of the shortwave cloud (Winton) and water vapor plus lapse rate feedbacks.

h. *Polar amplification contributions from HadSM3 experiments*

The overall polar amplifications for the HadSM3 experiments are given in Table 3. The +2% solar and LCscat experiments have similar NH polar amplification, and the $2 \times CO_2$ experiment has a slightly larger NH polar amplification. In the SH, the polar amplification is most similar for the $2 \times CO_2$ and LCscat experiments with the +2% solar experiment having the lowest polar amplification. The HCabs experiment has the largest polar amplification in both hemispheres by far. We do not show the polar amplification contributions from different feedbacks, forcing, and horizontal heat transport,

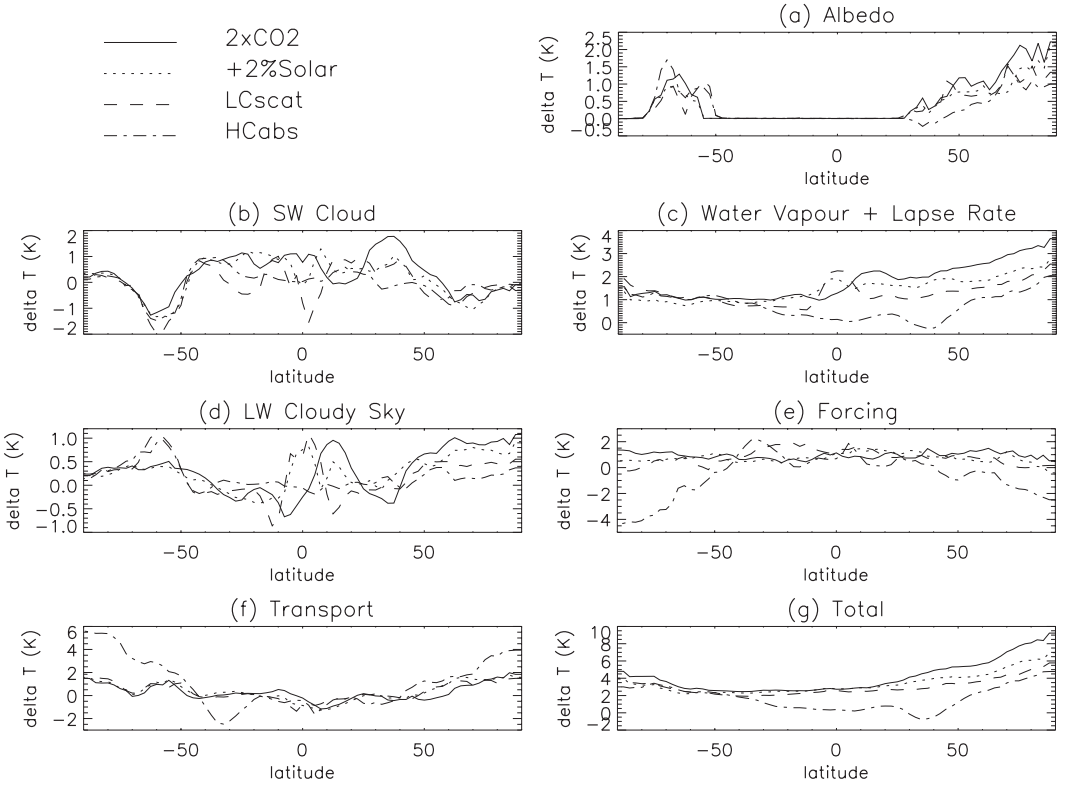

FIG. 10. Annual mean, zonal mean equilibrium partial temperature changes for HadSM3 experiments. Note that for LCscat and HCabs the temperature changes have been multiplied by −1 for ease of comparison with $2 \times CO_2$ and +2% solar.

but it is clear from Fig. 10 that in the HCabs experiment the horizontal heat transport plays a far more dominant role than in the other forcing mechanism experiments and the radiative forcing gives a strong negative contribution.

5. Conclusions

The eight different CMIP3 models forced with $2 \times CO_2$ that were analyzed show similar spatial patterns of feedback with similar seasonal behavior. The greatest intermodel differences are in the pattern of shortwave cloud and longwave cloudy-sky feedback in the tropics, in the water vapor plus lapse rate feedback in the tropics, and in the SH sea ice albedo feedback in summer. We find the greatest intermodel differences in the annual global mean equilibrium temperature response come from the water vapor plus lapse rate feedback followed by the shortwave cloud feedback, unlike Dufresne and Bony (2008) who found the cloud feedback had by far the greatest intermodel differences. Although in the annual mean the greatest contribution to polar amplification is from the albedo feedback, there is a strong coincident negative contribution from shortwave cloud feedback. Considerable positive contributions from the longwave cloudy sky feedback and the transport term occur in autumn and winter. The seasonal transport term includes both horizontal heat transport and heat storage and further study is required to separate these terms.

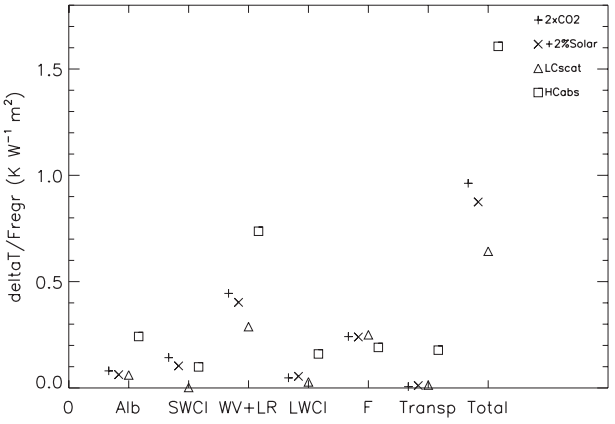

FIG. 11. Components of the climate sensitivity parameter for HadSM3 experiments. The climate sensitivity parameter is determined as annual mean, global mean equilibrium partial temperature changes (determined from zonal mean regression) divided by the global mean radiative forcing from regression.

TABLE 3. HadSM3 experiments equilibrium temperature response, regression forcing, climate sensitivity parameter ($\Delta T_{s,eq}/F_{regr}$), and polar amplification.

Forcing mechanism	Global mean ΔT_s at equilibrium (K)	Global mean forcing from regression $\pm 2\sigma$ (W m^{-2})	Climate sensitivity parameter (K W^{-1} m^2)	Annual mean NH polar amp [Eq. (13)]	Annual mean SH polar amp [Eq. (14)]
$2 \times CO_2$	3.52	3.66 ± 0.20	0.96	1.11	0.15
+2% solar	3.08	3.52 ± 0.33	0.87	0.77	−0.05
LCscat	−2.65	−4.13 ± 0.30	0.64	0.69	0.17
HCabs	−1.11	−0.69 ± 0.34	1.61	2.47	2.10

However, Lu and Cai (2009a) find the heat storage term to be only a secondary cause of the seasonality of polar amplification, although they do not separate out the heat transport term from longwave clear-sky terms. The greatest intermodel spread in the annual mean polar amplification is due to horizontal heat transport and shortwave cloud feedback and therefore a better understanding of these from observations may help constrain models, although due to large internal variability in the polar regions, this may be difficult (Stott and Jones 2009).

Spatial patterns of local climate feedback for a single model forced with four different forcing mechanisms having quite different radiative forcing patterns are quite similar. The equilibrium temperature response to high-level absorbing aerosol shows considerable differences compared to other forcing mechanisms in the contribution from horizontal heat transport and water vapor plus lapse rate feedback as well as from the forcing itself, leading to enhanced polar amplification and a greater climate sensitivity parameter.

Observations of the global mean temperature change and meridional temperature gradient trends over the twentieth century cannot be explained by greenhouse gas, solar, and ozone forcing alone. Shindell and Faluvegi (2009) use the residual to estimate sulfate (reflecting aerosol) and black carbon (absorbing aerosol) forcings over this time period. These estimated forcings are qualitatively consistent with historical emissions. Their calculations required the response per unit forcing for different forcing mechanisms in different regions, which they obtained from a single model. Since the mid-1970s the difference between the Arctic and SH extratropics temperature has been increasing. Shindell and Faluvegi (2009) suggest that ozone, black carbon, and the aerosol indirect effect have had a large impact on Arctic amplification owing to their inhomogeneous distribution. Although our absorbing aerosol experiment was not realistic, it shows that an inhomogeneous distribution of aerosols is not required to produce an inhomogeneous forcing or response, and that the response is strongly dependent on changes in heat transport and the associated amplification of feedbacks. Further work is still required to unravel the complex nature of aerosol forcing, the associated potentially strong semidirect effects, and the considerable changes to poleward heat transport before specific causes of recent Arctic temperature change can be confidently attributed.

Acknowledgments. We thank Gaby Rädel (Department of Meteorology, University of Reading, UK) for providing the instantaneous forcing data for the HadSM3 HCabs experiment and Lawrence Jackson (University of Leeds, UK) for advice on the regression statistics. We also thank several anonymous reviewers for their helpful comments on this manuscript. We acknowledge the modelling groups, the Program for Climate Model Diagnosis and Intercomparison (PCMDI) and the WCRP's Working Group on Coupled Modelling (WGCM) for their roles in making available the WCRP CMIP3 multimodel dataset. Support of this dataset is provided by the Office of Science, U.S. Department of Energy. This work was funded by NERC Grant "An Observationally-Based Quantification of Climate Feedbacks" NE/E016189/1. Nicola Stuber was supported by the EU Framework 6 Integrated Project QUANTIFY.

REFERENCES

Alexeev, V. A., P. L. Langen, and J. R. Bates, 2005: Polar amplification of surface warming on an aquaplanet in "ghost forcing" experiments without sea ice feedbacks. *Climate Dyn.,* **24,** 655–666.

Andrews, T., and P. M. Forster, 2008: CO_2 forcing induces semi-direct effects with consequences for climate feedback interpretations. *Geophys. Res. Lett.,* **35,** L04802, doi:10.1029/2007GL032273.

Boer, G. J., and B. Yu, 2003: Climate sensitivity and response. *Climate Dyn.,* **20,** 415–429.

Bony, S., and Coauthors, 2006: How well do we understand and evaluate climate change feedback processes? *J. Climate,* **19,** 3445–3482.

Cai, M., 2006: Dynamical greenhouse-plus feedback and polar warming amplification. Part I: A dry radiative-transportive climate model. *Climate Dyn.,* **26,** 661–675.

——, and J. Lu, 2007: Dynamical greenhouse-plus feedback and polar warming amplification, Part II: meridional and vertical asymmetries of the global warming. *Climate Dyn.,* **29,** 375–391.

Cess, R. D., and Coauthors, 1990: Intercomparison and interpretation of climate feedback processes in 19 atmospheric general circulation models. *J. Geophys. Res.,* **95,** 16 601–16 615.

——, and Coauthors, 1996: Cloud feedback in atmospheric general circulation models: An update. *J. Geophys. Res.,* **101,** 12 791–12 794.

Colman, R., 2002: Geographical contributions to global climate sensitivity in a general circulation model. *Global Planet. Change,* **32,** 211–243.

——, 2003: A comparison of climate feedbacks in general circulation models. *Climate Dyn.,* **20,** 865–873.

Dufresne, J.-L., and S. Bony, 2008: An assessment of the primary sources of spread of global warming estimates from coupled atmosphere–ocean models. *J. Climate,* **21,** 5135–5144.

Forster, P. M. F., and K. E. Taylor, 2006: Climate forcings and climate sensitivities diagnosed from coupled climate model integrations. *J. Climate,* **19,** 6181–6194.

——, M. Blackburn, R. Glover, and K. P. Shine, 2000: An examination of climate sensitivity for idealised climate change experiments in an intermediate general circulation model. *Climate Dyn.,* **16,** 833–849.

——, and Coauthors, 2007: Changes in atmospheric constituents and in radiative forcing. *Climate Change 2007: The Physical Science Basis,* S. Solomon et al. Eds., Cambridge University Press, 129–234.

Graversen, R. G., and M. Wang, 2009: Polar amplification in a coupled climate model with locked albedo. *Climate Dyn.,* **33,** 629–643.

Gregory, J., and M. Webb, 2008: Tropospheric adjustment induces a cloud component in CO_2 forcing. *J. Climate,* **21,** 58–71.

——, and Coauthors, 2004: A new method for diagnosing radiative forcing and climate sensitivity. *Geophys. Res. Lett.,* **31,** L03205, doi:10.1029/2003GL018747.

Hall, A., 2004: The role of surface albedo feedback in climate. *J. Climate,* **17,** 1550–1568.

Hansen, J., M. Sato, and R. Ruedy, 1997: Radiative forcing and climate response. *J. Geophys. Res.,* **102,** 6831–6864.

——, and Coauthors, 2005: Efficacy of climate forcings. *J. Geophys. Res.,* **110,** D18104, doi:10.1029/2005JD005776.

Holland, M. M., and C. M. Bitz, 2003: Polar amplification of climate change in coupled models. *Climate Dyn.,* **21,** 221–232.

Joshi, M., K. Shine, M. Ponater, N. Stuber, R. Sausen, and L. Li, 2003: A comparison of climate response to different radiative forcings in three general circulation models: Towards an improved metric of climate change. *Climate Dyn.,* **20,** 843–854.

Lohmann, U., and Coauthors, 2010: Total aerosol effect: Radiative forcing or radiative flux perturbation? *Atmos. Chem. Phys.,* **10,** 3235–3246.

Lu, J., and M. Cai, 2009a: Seasonality of polar surface warming amplification in climate simulations. *Geophys. Res. Lett.,* **36,** L16704, doi:10.1029/2009GL040133.

——, and ——, 2009b: A new framework for isolating individual feedback processes in coupled general circulation climate models. Part I: Formulation. *Climate Dyn.,* **32,** 873–885.

Meehl, G. A., and Coauthors, 2007: Global climate projections. *Climate Change 2007: The Physical Science Basis,* S. Solomon et al., Eds., Cambridge University Press, 747–845.

Qu, X., and A. Hall, 2006: Assessing snow albedo feedback in simulated climate change. *J. Climate,* **19,** 2617–2630.

Rap, A., P. M. Forster, A. Jones, O. Boucher, J. M. Haywood, and R. R. De Leon, 2010: Parameterisation of contrails in the UK Met Office climate model. *J. Geophys. Res.,* **115,** D10205, doi:10.1029/2009JD012443.

Shindell, D., and G. Faluvegi, 2009: Climate response to regional radiative forcing during the twentieth century. *Nat. Geosci.,* **2,** 294–300.

Shine, K. P., J. Cook, E. J. Highwood, and M. M. Joshi, 2003: An alternative to radiative forcing for estimating the relative importance of climate change mechanisms. *Geophys. Res. Lett.,* **30,** 2047, doi:10.1029/2003GL018141.

Soden, B. J., A. J. Broccoli, and R. S. Hemler, 2004: On the use of cloud forcing to estimate cloud feedback. *J. Climate,* **17,** 3661–3665.

——, I. M. Held, R. Colman, K. M. Shell, J. T. Kiehl, and C. A. Shields, 2008: Quantifying climate feedbacks using radiative kernels. *J. Climate,* **21,** 3504–3520.

Stott, P. A., and G. S. Jones, 2009: Variability of high latitude amplification of anthropogenic warming. *Geophys. Res. Lett.,* **36,** L10701, doi:10.1029/2009GL037698.

Trenberth, K. E., and Coauthors, 2007: Observations: Surface and atmospheric climate change. *Climate Change 2007: The Physical Science Basis,* S. Solomon et al., Eds., Cambridge University Press, 235–336.

Williams, K. D., C. A. Senior, and J. F. B. Mitchell, 2001: Transient climate change in the Hadley Centre models: The role of physical processes. *J. Climate,* **14,** 2659–2674.

——, W. J. Ingram, and J. M. Gregory, 2008: Time variation of effective climate sensitivity in GCMs. *J. Climate,* **21,** 5076–5090.

Winton, M., 2006a: Surface albedo feedback estimate for the AR4 climate models. *J. Climate,* **19,** 359–365.

——, 2006b: Amplified Arctic climate change: What does surface albedo feedback have to do with it? *Geophys. Res. Lett.,* **33,** L03701, doi:10.1029/2005GL025244.

Zhang, M. H., J. J. Hack, J. T. Kiehland, and R. D. Cess, 1994: Diagnostic study of climate feedback processes in atmospheric general circulation models. *J. Geophys. Res.,* **99,** 5525–5537.